

INTERACTION OF LASER RADIATION WITH MATTER

https://doi.org/10.1070/QEL16508

Ablation of steel under surface irradiation by high-intensity tandem pulses

V.V. Kononenko, V.I. Konov

Abstract. **Specific features of interaction of high-intensity (10^{15} W cm^{-2}) femtosecond laser pulses with ablated vapour are experimentally studied under a tandem (double pulse) regime of irradiation with a short (Δt = 1–11 ns) delay between the pulses. Using interference and shadow photography at a time scale of below 10 ns, data on dynamics of vapour expansion are obtained and the electron density in vapour is estimated. Reasons for observed strong screening of the radiation of the second pulse in a tandem are discussed.**

Keywords: *femtosecond laser radiation, metal surface ablation, high-repetition-frequency lasers.*

1. Introduction

Laser ablation is used in metal treatment (cutting, drilling, cleaning, structuring, etc.) [1] and producing new materials and structures (film deposition, elemental analysis, laser transfer, etc.) [2]. A natural request for a higher efficiency initiates improvement of laser systems by increasing the pulse repetition rate f and average output power. Presently, pulsed power supplies are developed with a peak power of above 12 MW [3] operating at $f \leqslant 100$ MHz [3, 4].

Obviously, the effects of residual excitation, which need to be considered in the high-frequency ablation, are thermal energy accumulation in the target that has not enough time to cool and interaction of ablated vapours with a jet that has no time to relax between pulses. Presently, ablation and gas-dynamics of target vapours are sufficiently well studied in a single-pulse regime of irradiation [5–7] including ultrashort pulses [8–11]. It is well known that in the process of surface treatment of solids, residual effects substantially influencing the established ablation regime begin to reveal already at relatively low ($f \approx 4$ kHz) frequencies [12]. In addition, there is a great number of works on investigating high-frequency ablation of conducting [13] and nonconducting [14, 15] materials at relatively low (below the threshold of a single-pulse ablation) irradiation intensities, where the key factor is heat accumulation in the irradiation zone. However, there are few experimental data on very high frequency ablation at intensities of above 10^{14} W cm^{-2}. At so high intensity, air breakdown occurs even without target and, obviously, the key factor becomes nonlinear processes in absorption of radiation in the jet of material ablated by a previous pulse [16].

The present work is devoted to studying specific features of interaction of high-intensity ($\sim 10^{15}$ W cm^{-2}) femtosecond tandem pulses imitating very high frequency ($\sim$100 MHz) irradiation of a steel surface with the laser jet. The effect of substantial (almost total) termination of metal removal by the second pulse in the tandem, which is explained by light absorption and scattering in plasma, is discovered.

2. Experiment

A system used in experiments comprised a Ti:sapphire laser (Tsunami, Spectra Physics, the radiation wavelength is 800 nm) and a regenerative amplifier (Spitfire, Spectra Physics), which provided a train of 100-fs pulses with a maximum energy of 1 mJ at a pulse repetition rate of 1 kHz. Visualisation of the results of interaction was realised by the 'probe beam' method (Fig. 1). After splitting into the main and probe beams, the main part of radiation (the exciting

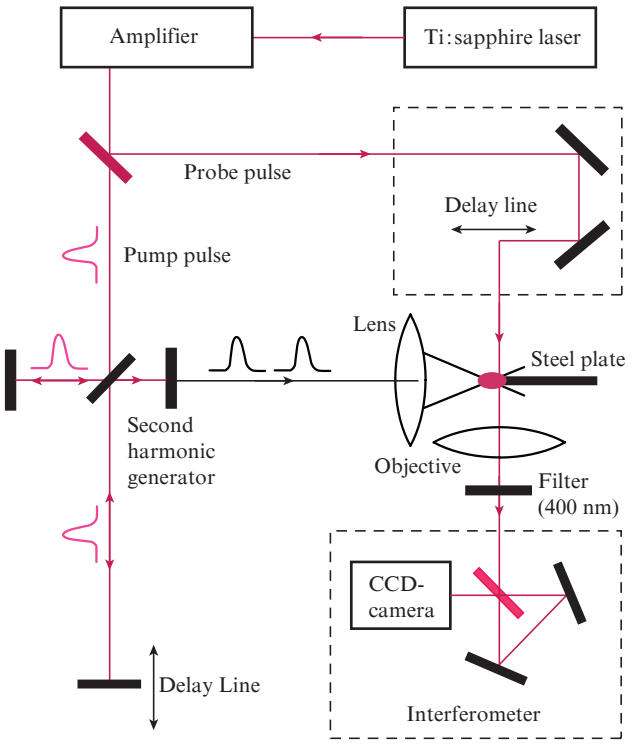

Figure 1. Schematic of the experimental setup.

V.V. Kononenko, V.I. Konov A.M. Prokhorov General Physics Institute, Russian Academy of Sciences, ul. Vavilova 38, 119991 Moscow, Russia; National Research Nuclear University 'MEPhI', Kashirskoe shosse 31, 115409 Moscow, Russia;
e-mail: vitali.kononenko@nsc.gpi.ru

Received 30 August 2017; revision received 17 October 2017
Kvantovaya Elektronika **48** (1) 40–44 (2018)
Translated by N.A. Raspopov

beam) passed again through a semitransparent (50%) mirror, which formed tandem pulses of equal energy. The variation of the time delay between the pulses in a wide range (up to dozens nanoseconds) allowed us to model the regime of very high frequency (above 100 MHz) irradiation by pulses with a sufficiently high intensity. Then the radiation was focused to a sample surface by a spherical lens ($F = 16$ mm).

The probe beam passed through a delay line and illuminated the jet from one side. An image of the domain subjected to intensive laser action was projected onto the entry plane of a CCD-matrix with magnification of about $30^{\times}$. Then the image was converted to a digital form and processed for obtaining information about the state of material in the irradiated zone. To minimise distortions introduced by diffraction of the probe beam at the edge of the sample, the latter had the form of a plate (steel foil) of thickness as small as 5–10 μm. In this configuration, radiation of the main beam undergoes substantial scattering and, having passed to the objective aperture, prevents observation. To avoid this, the pump radiation was converted to the second harmonic in front of a collective lens. Then the scattered light of the second harmonic was filtered in the channel of the probe beam.

The intensity distribution in the narrowest part of the laser beam waist was studied at low ($\sim$1 J cm^{-2}) energy densities, in which case nonlinear transformations of the beam were absent. In these conditions, craters were formed on a surface of the sample possessing a high linear absorption (amorphous carbon) at varied pulse energy. The diameter of a Gaussian beam determined from analysis of the dependence of crater diameters on the pulse energy was about 4 μm with respect to the level 1/e. In experiments with tandem irradiation, the pulse energy was 10 μJ. Hence, in vacuum, the energy density at the optical axis for the pulses specified reached $\sim$100 J cm^{-2} ($\sim 10^{15}$ W cm^{-2}).

Information about the state of matter in the process of laser action and after it was mainly obtained by the methods of femtosecond interferometry thoroughly described in [17] and shadow photography. Note that the two interference (or shadow) images were recorded each time in given irradiation conditions: with the excitation pulse (information image) and without it (background image). The difference image calculated on a PC comprised only the dynamic information, that is, information about the result of laser action, reducing in this way an image noise. Note that all static information was lost in this case, and the background was uniformly grey regardless of whether the sample masked the illumination beam at a particular point or not. However, the sample edge was always clearly distinguished in images because of the small shift in space due to mechanical vibrations.

The two complementary approaches were employed: 1) the method of femtosecond photography was used for studying the dynamics of relaxation of vapour plasma produced by a single laser pulse; and 2) the features of the ionisation of evaporated metal by two pulses with the time delay varied in the range 1–10 ns were studied, which allowed one to estimate in the first approximation the effect of high-frequency laser irradiation.

3. Results and discussion

The method for obtaining a difference image described above made it possible to measure the depth of the ablated channel directly in the process of irradiation. Under the multi-pulse laser action, the images show a local perturbation arising at the optical axis and moving inwards the sample in the process of irradiation. Figure 2 shows a series of images of an irradiated steel plate and a laser jet over its end surface, corresponding to various stages of channel formation at a low pulse repetition rate. The artefact mentioned is well seen in Fig. 2b. At early ablation stages (Fig. 2a), it is masked by a strong perturbation on the surface, at late stages (Fig. 2c) it penetrates deeper into the target and leaves the observation domain. We believe that the position of this artefact coincides with the current position of channel bottom. It arises because the shock wave generated in the ablation zone propagates not only in the ambient atmosphere, but also in metal itself. Finally, the perturbation of material density reaches the side surface of the plate and locally changes its properties, in particular, the coefficient of scattering, which makes it possible to fix the artefact on the surface visually. Note that the perturbed part is revealed at the delay between the exciting and

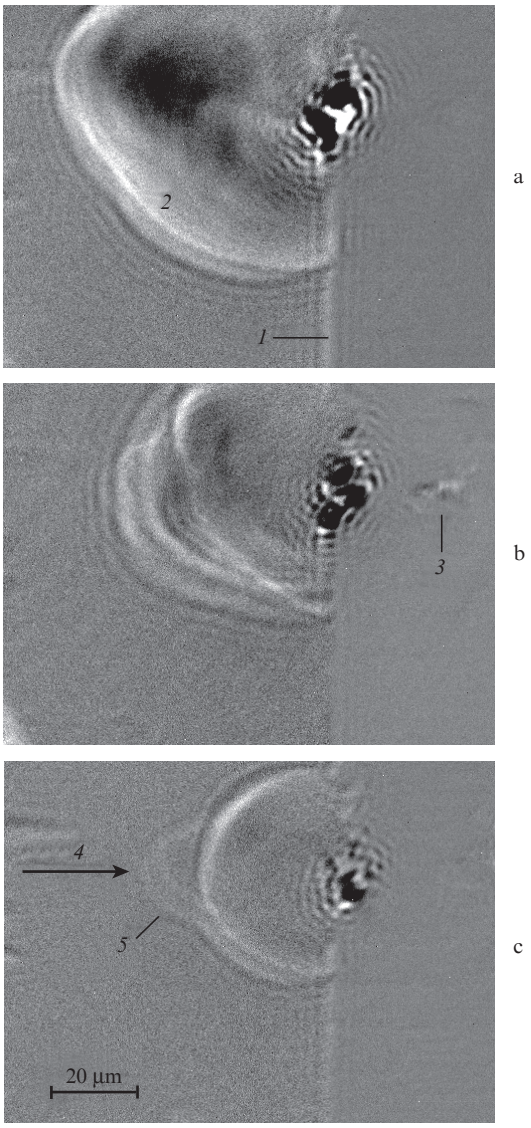

Figure 2. Shadowgraphs of the laser jet in a single-pulse regime of irradiation after (a) 10 pulses (a crater depth is 2 μm), (b) 90 pulses (27 μm) and (c) 800 pulses (40 μm). The delay between the pump pulse and probe pulse is 11 ns; (*1*) sample surface, (*2*) jet, (*3*) position of the channel bottom, (*4*) laser radiation propagation direction, (*5*) air breakdown.

illuminating pulses of 1 ns and more. At the delay of 10 ps, the artefact was not observed because, obviously, the front of a shock wave had not time enough to cover the distance of several micrometers and reach the surface.

Dependences of the crater depth in a steel plate on the number of irradiation cycles are shown in Fig. 3 for the single-pulse and tandem regimes of irradiation. Here, by the 'irradiation cycle' is meant either a single laser pulse, or tandem pulses. It was mentioned that the delay between the pulses in a tandem varied in the range 1–11 ns. Regardless of this parameter, there was no substantial difference in the ablation rates for the single-pulse and tandem regimes of irradiation. Obviously, it means that all the energy of the second pulse is completely absorbed in the laser jet, produced by the first pulse, and the radiation does not reach the target surface. Note that the dynamics of growing crater depth is quite typical: it has a linear character until the crater is shallow, and then the rate of ablation falls to zero.

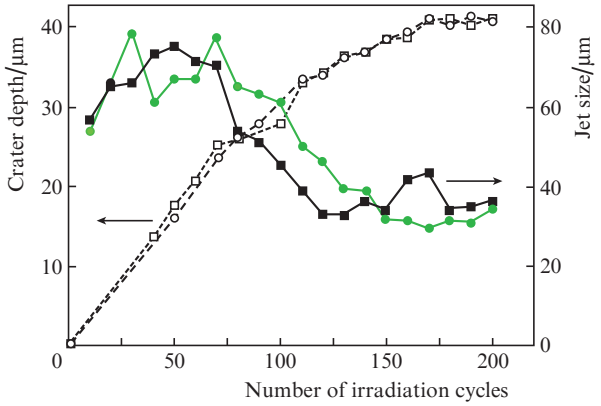

Figure 3. Crater depth in steel and jet size over sample surface vs. the number of irradiation cycles in the single-pulse (squares) and tandem (circles) regimes. The delay between pulses in the tandem regime is 11 ns.

Note also that a substantial broadening of obtained channel was observed in the tandem regime as compared to single-pulse regime. In our experiments, it was 50%–100% and, obviously, the reason was erosive etching by plasma of iron vapours ionised and heated by the second pulse.

The full screening observed for the second pulse in a tandem and erosive etching of channel walls by plasma confirm the initial assumption that at radiation intensities of $\sim 10^{15}$ W cm^{-2} the key factor determining physics of laser pulse interaction with matter at very high pulse repetition rates is the residual excitation of substance in the irradiation zone. Here, 'excitation' means a laser-induced change of the state of target material, first of all, the state of a vapour jet: the density, temperature and degree of ionisation. Understanding specific features of high-frequency pulsed laser treatment requires thorough information about relaxation processes in a jet.

One should take into account that even at a low pulse repetition rate the result of laser radiation action on a target strongly depends on the surface morphology formed by previous pulses. Already in a relatively shallow crater (about several crater diameters), the irradiation conditions strongly differ from the case of the initial plane surface. When the aspect ratio for the ablated channel reaches 10, the effects of waveguide propagation begin to reveal, which changes the interaction conditions even more. Thus, in the process of channel growing in target, the laser jet parameters dynamically change [18], which can substantially complicate the picture under high-frequency excitation.

This relationship between the properties of laser jet and channel geometry is clearly demonstrated in Fig. 3, where dependences of a laser jet longitudinal dimension are presented versus the number of irradiation cycles. One can clearly see that dynamics of the crater depth correlates with the laser jet dimension. At greater depth, the distance to which vapours spatter in a time lapse between the exciting and probe pulses (11 ns) becomes shorter. Actually, such a collapse of the laser jet is expected; it shows that even if a deep channel is irradiated, the jet is formed mainly at the channel bottom, and the shock wave needs some time to get the target surface and start expansion to ambient space.

Note that motion of the ablation zone inwards the target allows one to observe air breakdown in a laser caustic over the surface (see Fig. 2c). It is specific in the absorption of the radiation energy along the laser caustic and in the shape of the cloud of plasma diffusion expansion, which is close to elliptical [19]. In the case of radiation absorption in target, the ablated material expands from a point forming a hemispherical shock wave. This distinction in geometry allows one to distinguish the air breakdown from target vapour jet (see Fig. 2c).

A sufficiently complicated process of vapour expansion results in a linear dependence of the longitudinal jet size on time (Fig. 4). However, this dependence cannot be obtained in the frameworks of the model of simple successive motion of a shock-wave front first through the channel and then isotropicly into ambient space. Nevertheless, on a surface, the experimental dependence of the spark length on time can be satisfactorily described by the curve of the type $R(t) \sim t^{2/5}$ (Fig. 4). This dependence is predicted by the point explosion model [20]: $R(t) \sim t^a$, where $a = 2/5$ occurs at instant energy release at a point – the case of spherical symmetry, which, obviously, is closest to our conditions. All previously discussed testifies that ablation in a deep channel is not totally localised at a single point, in particular, at the channel bottom. Correspondingly, formation of a laser jet with the following gas-dynamic expansion has very complicated character.

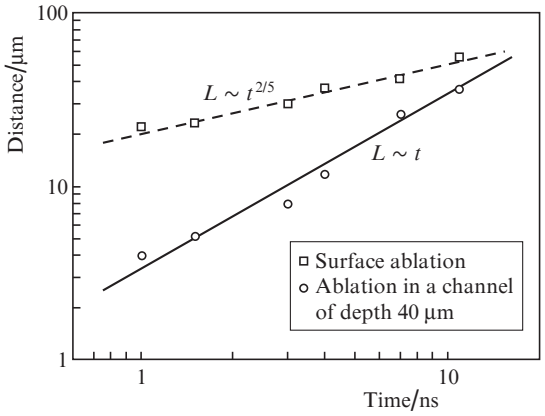

Figure 4. Time evolution of the longitudinal size of a laser jet obtained in the single-pulse irradiation regime: for the first pulse – ablation on the surface, for 200th pulse – ablation in a channel of depth ~40 μm.

It is quite difficult to study the formation of the laser jet in a channel, its relaxation and interaction with laser radiation not only because of the numerous processes involved, but also because it is appreciably localised deep in a nontransparent target. This problem is resolved in the case of surface ablation, which gives a principal possibility to use femtosecond interferometry for obtaining information about jet properties, dynamics and absorbed energy. Figure 5 presents interference images of a laser jet obtained in the single-pulse and tandem regimes within 11 ns after the first laser pulse reaches the surface. The second pulse in the tandem arrives directly prior to the probe pulse (in approximately 1 ps); hence, the processes of recombination and gas-dynamic expansion can be neglected in the excitation induced by this pulse (Fig. 5b).

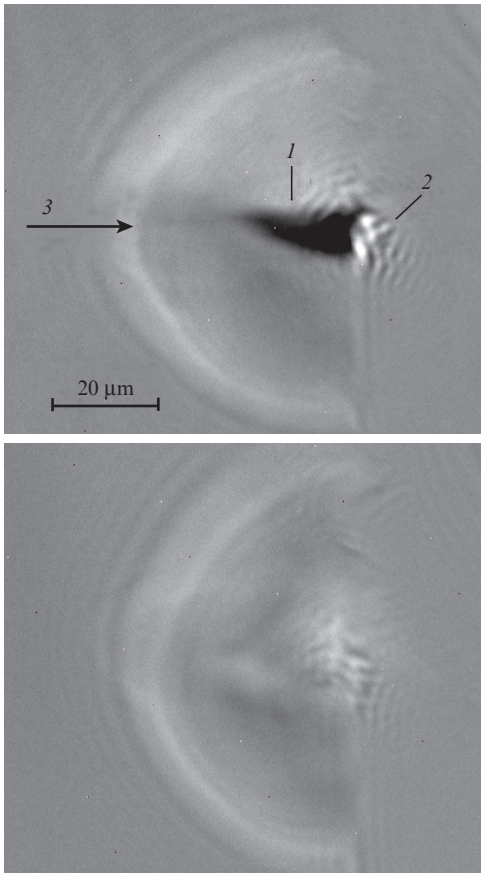

Figure 5. Interference image of a jet of ablated vapours as a result in the irradiation regimes of (a) single-pulse and (b) tandem with a delay of 11 ns; (*1*) ionisation of jet vapours; (*2*) low-temperature vapour component, (*3*) propagation direction of the laser radiation.

Issuing from the Drude high-frequency conduction model and given Δn (variation of the refractive index in jet for the electromagnetic wave with frequency ω) we can estimate the concentration of free carriers in plasma: $N \approx m_e\omega^2\Delta n/(2\pi e^2)$, where e and m_e are the electron charge and mass, respectively. Analysis of the interference images shows that due to expansion and cooling of the laser jet formed by the first pulse and to recombination processes in jet, in a time moment of 11 ns the concentration of free electrons does not exceed $10^{17}-10^{18}$ cm^{-3}. In this case, metal evaporated by one pulse and expanded to this instant in the form of vapour to a hemisphere of radius ~50 μm, forms a cloud with the iron atomic concentration of $\sim 10^{19}$ cm^{-3}. The concentrations of electrons and iron ions in the vapour are close to those observed under femtosecond air breakdown in a laser spark [19], however, with a substantial distinction. In the gas breakdown, the diffuse expansion of plasma leads to a sharp fall of substance density in it, which is the reason for abrupt reduction in the efficiency of material ionisation by subsequent pulses – there is nothing to be ionised. In the case of femtosecond ablation, there is an 'injection' of the substance evaporated from a target surface, and so the efficiency of a second laser breakdown does not fall, at least for a time moment of 11 ns.

The image of the plasma jet produced by the second pulse in a tandem (Fig. 5b) clearly demonstrates this fact. Plasma arises just after the action of the second pulse with an electron concentration $N \approx 10^{19}$ cm^{-3}, that is, all atoms of iron vapours are ionised. Nevertheless, these observations do not give an answer to the question where the energy of the second pulse disappears since ablation from the second pulse is lacking.

Indeed, after the 11-ns relaxation, metal vapours are actually transparent for the radiation. Interaction of the second pulse with the plasma induced by it also cannot be substantial. One can derive this conclusion just by analogy to the features of femtosecond single-pulse air breakdown, where interaction with gas medium of the same density leads to the same degree of ionisation. The value of nonlinear scattering in far zone measured in [21] is substantial ~50%, which, however, does not explain the degree of screening observed. As well, simple estimates show that already at the minimal temperature found in the literature for ionised metal vapours ($T \approx 1$ eV [22, 23]), the depth of field penetration to such plasma is ~10 μm. This agrees with the observation made in the present work: while a pulse propagates along the optical axis, the absence of the gradient of carrier concentration in this direction (Fig. 5b) testifies that there is no tendency to reduce the ionisation efficiency, which means the relatively weak dissipation of radiation energy in jet.

The absence of ablation under the action of the second pulse cannot be explained by energy loss to generation of soft X-ray radiation and higher harmonics in the plasma produced. The efficiency of these processes is relatively low. In gases, it usually does not exceed 10^{-5} [24]. One can hardly expect that in more dense plasma this value will substantially increase; thus, in considering ablation, these processes are usually neglected [25].

Strong screening of the radiation of the second pulse in a tandem can possibly be explained by its interaction not with strongly expanded vapours of the laser jet, but with the part of molecules, which are comprised in a low-energy 'tail' of the jet temperature distribution. The time interval of ~10 ns is not enough for such molecules to cover a substantial distance, and so these are localised near the surface. From Figs 2 and 5 one can see that in 11 ns after the first pulse, there is a strong perturbation at a distance of several microns from the surface. This perturbation is black on the shadow photograph and white on the interference image. It can be identified as a medium with a positive increment ($\Delta n \sim +0.03$) of the refraction index and optical density of ~3 at the probe beam wavelength of 800 nm. Issuing from the fact that the refraction index for metal vapours at normal pressure is ~1.001 [26], for a 30-times more dense vapour we obtain a medium with n close to the measured value. Absorption of the radiation energy in so dense gas ($N \sim 10^{21}$ cm^{-3}) may result in formation of a strongly absorbing plasma layer with a high density

(possibly, higher than the critical value), which can hardly be observed directly due to its small thickness.

4. Conclusions

In the present work, features of the laser ablation of steel surface by tandem pulses are experimentally studied at a high radiation intensity ($\sim 10^{15}$ W cm^{-2}). The maximal delay between the pulses in a tandem (11 ns) was chosen issuing from the record high pulse repetition frequency of powerful laser systems developed presently ($\sim$100 MHz). It was found that dynamics of crater depth growing (the rate of ablation) in the case of tandem pulses is just the same as for single pulses, which suggests that femtosecond radiation is totally screened by metal vapours. By using shadow and interference photography, the laser jet dynamics in a single-pulse regime was studied and it was shown that in a time lapse of $\sim$10 ns the density of hot vapours in the jet is $\sim 10^{19}$ cm^{-3}, and the degree of ionisation is relatively low (1%–10%). Thus, the radiation of the following pulse cannot be substantially screened. It was found that in these conditions at a small distance ($\sim$1 μm) from the surface, the vapour concentration reaches $\sim 10^{21}$ cm^{-3}, which may lead to the strong screening observed. In this case, the second pulse does not reach the surface of the solid because all its energy is absorbed or even reflected when the density of plasma is above the critical value. An interesting feature of crater formation in the considered conditions is intensive erosive etching of crater walls by this plasma, which results in a substantial broadening of the channel in the tandem irradiation regime as compared to the single-pulse regime.

Acknowledgements. The work was supported by the Ministry of Education of the Russian Federation (Project No. 3.2608.2017/PCh).

References

1. Rubahn H.-G. *Laser Applications in Surface Science and Technology* (New York: John Wiley & Sons, 1999).
2. Eason R. *Pulsed Laser Deposition of thin Films: Applications-led Growth of Functional Materials* (New York: John Wiley & Sons, 2007).
3. Tunnermann A., Wirth C., Seise E., Limpert J., Hanf S., Gabler T., Schreiber T., Andersen T.V., Eidam T. *Opt. Lett*., **35**, 94 (2010).
4. Song R., Hou J., Chen S., Yang W., Lu Q. *Appl. Opt*., **51**, 2497 (2012).
5. Askaryan G.A., Rabinovich M.A., Savchenko M.M. *Pis'ma Zh. Eksp. Teor. Fiz*., **5**, 150 (1967).
6. Prokhorov A.M., Konov V.I., Ursu I., Michelesku I.N. *Vzaimodeistvie lazernogo izlucheniya s metallami* (Interaction of Laser Radiation with Metals) (Moscow: Nauka, 1988).
7. Anan'in O.B., Afanas'ev Yu.V., Bykovskii Yu.A., Krokhin O.N. *Lazernaya plazma. Fizika i primeneniya* (Laser Plasma. Physics and Applications) (Moscow: Izd. MEPhI, 2003).
8. Zergioti I., Stuke M. *Appl. Phys. A*, **67**, 391 (1998).
9. Schmidt V., Husinsky W., Betz G. *Phys. Rev. Lett*., **85**, 3516 (2000).
10. Amoruso S., Wang X., Altucci C., de Lisio C. *Appl. Surf. Sci*., **186**, 358 (2002).
11. Dausinger F. *Proc. SPIE*, **4830**, 471 (2003).
12. Klimentov S.M., Pivovarov P.A., Konov V.I., Brightling D., Dausinger F. *Quantum Electron*., **34**, 537 (2004) [*Kvantovaya Elektron*., **34**, 537 (2004)].
13. Rode A.V., Luther-Davies B., Gamaly E.G. *J. Appl. Phys*., **85**, 4222 (1999).
14. Schaffer C.B., Garcia J.F., Mazur E. *Appl. Phys. A*, **76**, 351 (2003).
15. Luther-Davies B., Rode A.V., Madsen N.R., Gamaly E.G. *Opt. Eng*., **44**, 051102 (2005).
16. Lapczyna M., Chen K.P., Herman P.R., Tan H.W., Marjoribanks R.S. *Appl. Phys. A*, **69**, S883 (1999).
17. Kononenko V.V., Zavedeev E.V., Latushko M.I., Pashinin V.P., Konov V.I., Dianov E.M. *Quantum Electron*., **42**, 925 (2012) [*Kvantovaya Elektron*., **42**, 925 (2012)].
18. Garnov S.V., Klimentov S.M., Konov V.I., Kononenko T.V., Dausinger F. *Quantum Electron*., **28**, 42 (1998) [*Kvantovaya Elektron*., **25**, 45 (1998)].
19. Kononenko V.V., Kononenko T.V., Pashinin V.P., Gololobov V.M., Konov V.I. *Quantum Electron*., **43**, 356 (2013) [*Kvantovaya Elektron*., **43**, 356 (2013)].
20. Sedov L.I., Korobeinikov V.P., Markov V.V. *Trudy Matematicheskogo Instituta im. Steklova*, **175**, 178 (1986).
21. Klimentov S.M., Kononenko T.V., Pivovarov P.A., Garnov S.V., Konov V.I., Prokhorov A.M., Brightling D., Dausinger F. *Quantum Electron*., **31**, 378 (2001) [*Kvantovaya Elektron*., **31**, 378 (2001)].
22. Ye M., Grigoropoulos C.P. *J. Appl. Phys*., **89**, 5183 (2001).
23. Kononenko T.V., Valter D., Konov V.I., Dausinger F. *Quantum Electron*., **39**, 328 (2009) [*Kvantovaya Elektron*., **39**, 328 (2009)].
24. Kim I.J., Kim C.M., Kim H.T., Lee G.H., Lee Y.S., Park J.Y., Cho D.J., Nam C.H. *Phys. Rev. Lett*., **94** (24), 243901 (2005).
25. Choi T.Y., Grigoropoulos C.P. *J. Appl. Phys*., **92** (9), 4918 (2002).
26. Kikoin I.K. *Tablitsy fizicheskikh velichin* (Tables of Physical Values) (Moscow: Atomizdat, 1976).